Purdue University

Purdue e-Pubs

School of Aeronautics and Astronautics Faculty Publications

School of Aeronautics and Astronautics

2012

Nonlinear Effects in Squeeze Film Gas Damping on Microbeams

S Chigullapalli
Purdue University

A Weaver
Purdue University

Alina A. Alexeenko
Purdue University - Main Campus, alexeenk@purdue.edu

Follow this and additional works at: http://docs.lib.purdue.edu/aaepubs

Part of the Engineering Commons

Nonlinear Effects in Squeeze Film Gas Damping on Microbeams

S Chigullapalli, A Weaver and A Alexeenko

School of Aeronautics & Astronautics, Purdue University, West Lafayette, IN 47907

E-mail: `alexeenk@ecn.purdue.edu`

Abstract.

We consider squeeze film gas damping during microbeam motion away and toward a substrate as occurs during opening and closing of RF switches and other MEMS devices. The numerical solution of the gas damping problem in two-dimensional geometries is obtained based on the Boltzmann-ESBGK equation. The difference in damping force between downward and upward moving beams is shown to vary from as little from as 5% for low beam velocities of $0.1\,m/s$ to more than 200% at $2.4\,m/s$. For a constant velocity magnitude of $0.8\,m/s$, this difference increases from 60% to almost 90% when the pressure is reduced by an order of magnitude. The numerical simulations are consistent with earlier observations of a significantly higher damping force during the closing of a capacitive RF MEMS switch reported by Steeneken et al. (JMM, 15, 176-184, 2005). The physical mechanism leading to this non-linear dependence of the damping force on velocity has been attributed to the differences in the flow rarefaction regime for the gas in the microgap.

1. Introduction

Various micro-electro-mechanical system (MEMS) devices involve microstructures in large-displacement motion. Examples include accelerometers, RF switches and filters [1]. The dynamics these devices is governed by coupled mechanical, electrical and fluidic phenomena. As the device size decreases the surface forces such as fluid damping dominate over the volume forces such as inertia due to the large surface to volume ratio. Prediction of the gas damping force therefore is important for design of such moving microstructures. Of specific interest is the squeeze film damping, which is the force generated when gas is pushed to or pulled out in a thin gap of fluid between two structures in relative motion.

At low speeds, the gas flows is incompressible and can often be described by the Reynolds equation, a simplified form of the Navier-Stokes equations with negligible convective terms. Reynolds equation is often used to describe fluidic effects in microsystems with gas confined in long gaps. However, the Reynolds and Navier-Stokes description breaks down when the characteristic size decreases and the flow transitions to rarefied regime. The flow rarefaction is characterized by the Knudsen number, the ratio of the molecular mean free path (about $60\,nm$ at the standard atmosphere conditions) to the characteristic size of the problem, i.e. the gap between the moving structures. There are a number of gas-damping models[2, 3] developed for a variety of geometries and ranges of Knudsen numbers. Squeeze-film damping experiments conducted by Andrews et al. [4] and Sumali [5] were used to validate models based on the continuum Reynolds equation for rigid structures. Similarly, Nayfeh and Younis [6] developed a model for a flexible clamped-clamped beam and their calculations agreed well with experimental data obtained by Legtenberg and Tilmans [7]

Martin et al. [8] presented simple models for determining the damping of microcantilever, bridge, and paddle resonators in vertical, horizontal, and torsional motion, operating in the free-molecular-flow regime with validity up to velocities approaching 20% of thermal speed. The Boltzmann equation is a general form of the gas transport equation based on the kinetic theory and can be reduced to Navier-Stokes equations in the near-continuum, small Knudsen number limit. Based on the numerical solution of the Boltzmann ES-BGK equation, Guo and Alexeenko [9] developed a simple expression for damping coefficient that is valid through slip, transitional and free-molecular regime. However, all of these models are developed based on the assumption that the direction of beam motion does not affect the magnitude of resistance from the fluid.

The squeeze-film damping is often characterized by the value of the damping coefficient c_f and the quality factor Q_n defined as follows

$$c_f = \frac{F}{v_{beam}L} \tag{1}$$

$$Q_n = \frac{m\omega_n}{c_f} \tag{2}$$

$$\omega_n = \gamma_n^2 \sqrt{\frac{EI}{\rho_s b t L^4}} \tag{3}$$

where L, b, t are length, width and thickness, E is the Young's modulus and $I = bt^3/12$ is the area moment of inertia of the planar beam, n is the vibrational mode corresponding to the frequency ω_n. For MEMS dynamics models the frequently made assumption is that the velocity of the motion is small enough that the damping force depends linearly on the velocity. Thus the damping coefficient is constant with respect to velocity and the direction of beam motion does not affect the damping parameters.

Steeneken et al. [10] used a high time-resolution detection set-up to determine dynamics and gas damping force in a RF MEMS capacitive switch. They showed that the damping coefficient during switch closing was higher than that during the opening. In particular, during opening the damping force followed the slip-flow equation at small gaps and approached the no-slip flow curve at larger gaps. Our quasi-steady simulations show a similar trend with the damping force during closing is much higher than that during opening for the same velocity magnitude. The challenge of selecting an adequate description for gas damping in MEMS switches therefore consists in the fact that the Knudsen number, velocity magnitude, and velocity direction all vary during the switch operation. In this paper, we show the effects on the damping force for various beam velocities and two different Knudsen numbers from the numerical solution of Boltzmann model kinetic equations. The difference between the predicted damping forces for upward and downward moving beams is higher at larger beam velocities and higher Knudsen numbers. The effect of direction of motion of the beam on the convergence rate is explained in terms of local Knudsen number and entropy generation rate.

The remainder of the paper is organized as follows. Section 2 presents briefly the governing equations and numerical solution method for the gas damping simulations. Section 3 describes the geometry and simulation conditions. Finally in Section 4 we present results for 2D squeeze-film damping and show the effect of beam velocity magnitude and direction on the damping force calculated from numerical simulations. The simulation results are compared qualitatively with the experimental observations of damping force by Steeneken et al.[10].

2. Gas Damping Modeling Approach

The simulations of the gas damping are performed based on the Boltzmann-ESBGK model of rarefied gas flows as described below.

2.1. ES-BGK Equation

The full Boltzmann Model Kinetic equation in three dimensions is of the form:

$$\underbrace{\frac{\partial f}{\partial t}}_{Transient\ term} + \underbrace{c_x\frac{\partial f}{\partial x} + c_y\frac{\partial f}{\partial y} + c_z\frac{\partial f}{\partial z}}_{Convective\ term} = \underbrace{-\nu(f - f_\gamma)}_{Collision\ term} \tag{4}$$

The ellipsoidal-statistical model (ES-BGK), introduced by Holway [11] where the Maxwellian f_γ of the standard BGK model is replaced by an anisotropic Gaussian. This model can reproduce transport coefficients corresponding to arbitrary Prandtl numbers (Pr) while the standard BGK model gives a $Pr = 1$.

$$f_\gamma = \frac{\rho}{\sqrt{det(2\pi\mathbb{T})}}\ e^{\left[-\frac{1}{2}(\vec{c}-\vec{V})^T\mathbb{T}^{-1}(\vec{c}-\vec{V})\right]} \tag{5}$$

$$\vec{c} - \vec{V} = [c_x - u, c_y - v, c_z - w]$$
$$\rho\mathbb{T} = \frac{1}{Pr}\rho RTI + (1 - \frac{1}{Pr})\rho \ominus$$
$$\rho \ominus = <(\vec{c}-\vec{V})\otimes(\vec{c}-\vec{V})f>$$
$$\rho RTI = <(\vec{c}-\vec{V})\otimes(\vec{c}-\vec{V})f_{\gamma,BGK}>$$

where notation $<>$ denotes an expectation value and $\otimes$ denotes a tensor product. The ES-BGK collision term satisfies the conservation of mass, momentum and energy which may be written as

$$\int mSd\mathbf{c} = 0, \int mc_iSd\mathbf{c} = 0, \int \frac{m}{2}c^2Sd\mathbf{c} = 0$$

The production of entropy is always positive (H-theorem) as presented by Andries et al. [12],

$$-k\int \ln fSd\mathbf{c} \geq 0$$

A 2-dimensional explicit ES-BGK solver was developed in Ref. [18] and it was shown that Boltzmann model equations can provide a practical modeling framework for a wide range of Knudsen numbers. In this paper, we use an unsteady, unstructured 3D finite volume solver for all the simulations.

3. Numerical Method

The solver is based on the finite volume method in the physical space and the discrete ordinate method in the velocity space with an implicit time discretization. The velocity space discretization is implemented using both Cartesian type with uniform velocity abscissas and spherical type meshes up to 16th order Gauss-Hermit quadrature [14] in velocity magnitude and both $3/8^{th}$ rule and constant interval in angles. The Cartesian type consists of discretization A Cartesian mesh of size $10 \times 10 \times 10$ with a cut-off

of $c_{max} = 5.5$ was used in discretization of velocity mesh for all simulations in this paper.

The macroparameters such as density, velocity and temperature are then calculated as:

$$\rho \quad = \sum_j f_j w_j \tag{6}$$

$$\rho \vec{V} \quad = \sum_j \vec{c} f_j w_j \tag{7}$$

$$\frac{3}{2}\rho T = \sum_j \left((c_x - u)^2 + (c_y - v)^2 + (c_z - w)^2\right) f_j w_j \tag{8}$$

where w_j is the weight associated with the jth ordinate in velocity space.

The discretization in the physical space is based on arbitrary finite volume meshes. CuBit and Gambit were used to create the various meshes for the different tests. The solver has capability to read the input files from aforementioned grid generators and partitions them by using ParMETIS (parallel version of METIS) [20] to create local meshes. Starting with the full 3D ESBGK equation:

$$\underbrace{\frac{\partial f}{\partial t}}_{Transient\ term} + \underbrace{c_x \frac{\partial f}{\partial x} + c_y \frac{\partial f}{\partial y} + c_z \frac{\partial f}{\partial z}}_{Convective\ term} = \underbrace{-\nu(f - f_\gamma)}_{Collision\ term} \tag{9}$$

The ESBGK equation for each discrete velocity ordinate c_j is written in the form of a linear system. An algebraic multigrid solver (AMG)[16, 17] is used for the solution of these linearized equations [15]. Details for discretization of the different terms, algorithm for implementation of Dirichlet and extrapolation conditions can found in Ref [15]. For all the steady 2D simulations the linear system is automatically set-up to solve the equivalent equation:

$$\underbrace{c_x \frac{\partial f}{\partial x} + c_y \frac{\partial f}{\partial y}}_{2D-Convective\ term} = \underbrace{-\nu(f - f_\gamma)}_{Collision\ term} \tag{10}$$

Following the discrete velocity approach suggested by Mieussens [13], the function $f_\gamma(x_i, t_k, c_j)$ for the BGK type equilibrium equation is chosen in the form

$$f_\gamma = \alpha_1 e^{\beta \cdot \mathbf{p}} \tag{11}$$

$$\beta = [-\alpha_2, \alpha_3, -\alpha_4, \alpha_5, -\alpha_6, \alpha_7, \alpha_8, \alpha_9, \alpha_{10}] \tag{12}$$

$$\mathbf{p} = [(c'_x)^2, c'_x, (c'_y)^2, c'_y, (c'_z)^2, c'_z, c_x c_y, c_y c_z, c_z c_x]^T \tag{13}$$

where $c'_x = c_x - u, c'_y = c_y - v, c'_z = c_z - w$ represent the thermal velocities. The coefficients (α_s) can be found from the discrete set of mass, x-momentum, y-momentum, z-momentum and energy conservation equations and are solved iteratively using the Newton's method. For detailed description of the conservative discretization of the collision term, linearization of the ES-BGK equations and boundary conditions please see Ref. [21].

4. Simulation Setup

All 2D damping simulations were performed on RF MEMS switch. The electroplated Nickel fixed-fixed beam has dimensions of $400\,\mu m$ length, $120\,\mu m$ width and $2\,\mu m$ thickness. The 2D slice of the beam considered here is at a gap size of $3.52\,\mu m$. Due to the symmetry of the problem only half of the beam is modeled. The top and right boundaries are open to free stream air and thus are designated as pressure inlets. Wall boundary conditions (BC) are applied to the bottom substrate and the beam boundaries. Figure 1 indicates these boundary conditions. To setup the simulations, spatial meshes were constructed and nominal grid sizes were determined through Richardson Extrapolation (RE). Solution dependence on velocity space and unsteady effects are also investigated.
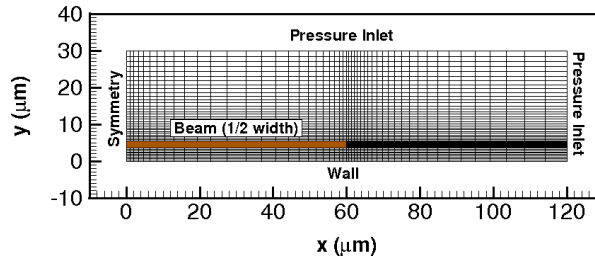
Figure 1. Nominal 50x50 mesh and applied BC's

Spatial grid convergence study was performed for a downward beam with highest velocity of $2.44\,m/s$ at $0.1\,atm$. Spatial grids of sizes 50×50 and 100×100 result in approximately 9% and 2% higher damping forces respectively when compared to value from Richardson's Extrapolation (RE). The effect of velocity space discretization on the damping force calculations has been studied for the same case. A Cartesian mesh of size 20^3 and a spherical mesh of size $8 \times 32 \times 16$, i.e., 8th order accurate with 32 and 16 constant angles in θ and ϕ, result in nearly identical damping forces, however the Cartesian mesh requires more than twice the computational time. Using a coarser Cartesian mesh of size 10^3 results in approximately 5% higher damping force than that computed from the other discretizations. This mesh is computationally least expensive taking only half the computational time as a spherical mesh and therefore has been used for all simulations in this paper.

Unsteady effects are investigated to ensure numerical accuracy of steady state iterations to convergence. A transient simulation of a beam moving at $-0.8\,m/s$ using a dimensional time-step of $6.25 \times 10^{-3}s$ resulted in identical damping force and pressure fields as shown in Fig. 2. However, the time taken for a transient simulation is 38 hours while it is only 24 hours for the steady simulation. As such, for the remainder of the paper, solutions from steady state simulations are used.
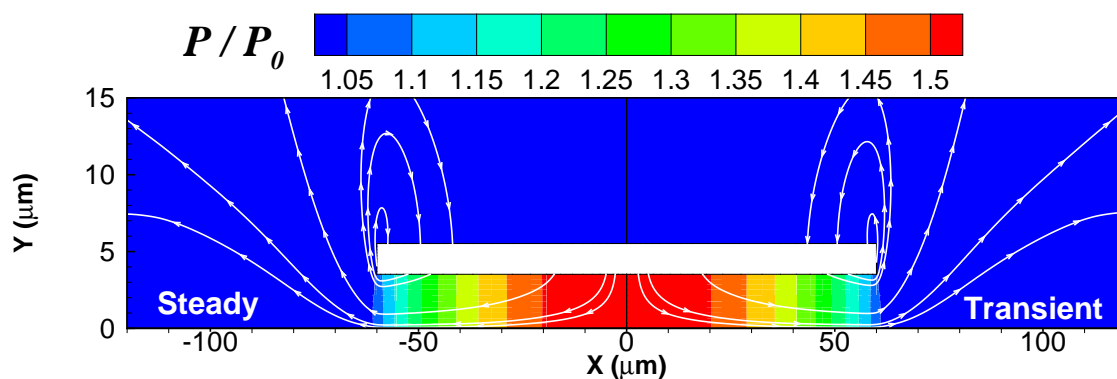
Figure 2. Transient vs. steady state comparisons for beam velocity of $-0.8\,m/s$

5. Results and Discussion

Damping forces for an upward and downward moving beam as well as pressure fields, local Knudsen numbers, and gas flow velocities are obtained from the ES-BGK simulations. Figure 3 shows pressure contours for upward and downward moving beams at the highest and lowest velocities of $0.8\,m/s$ and $2.44\,m/s$. The non-dimensional pressure ranges from 1.35 to 0.8 for $V = 0.8\,m/s$ and from 3.4 to 0.6 at $V = 2.44\,m/s$. Therefore the fluid is compressed at least three times more for a downward moving beam at higher velocity. However the fluid is rarefied only a little more for an upward moving beam at the higher velocity. Therefore at high velocities, the difference between magnitude of the damping force is very high and sometimes over 200% as shown in the next subsection.
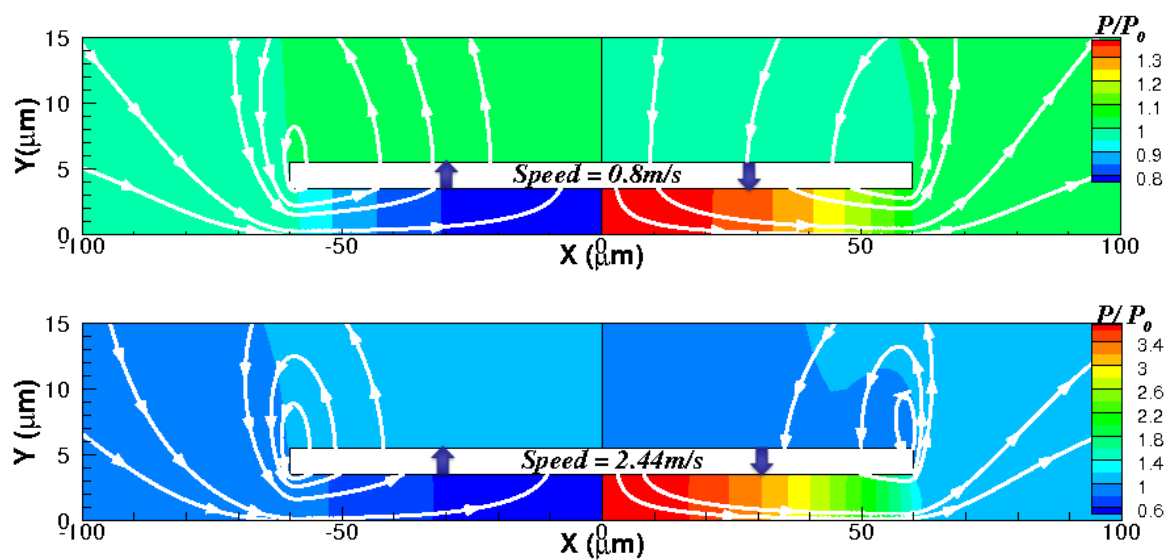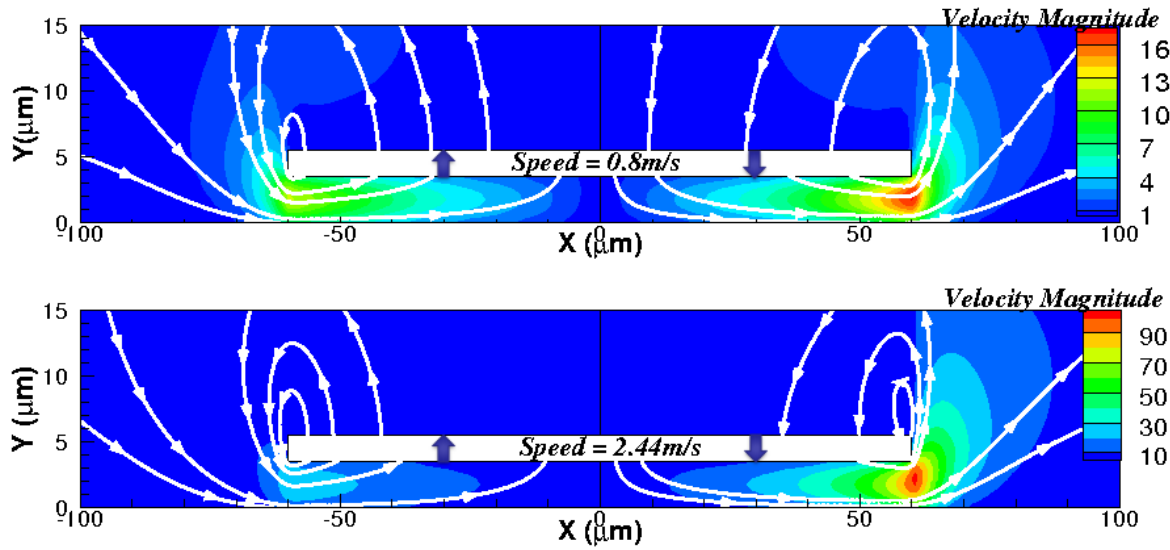

Figure 3. Pressure contours for varying beam direction of motion for $V = 0.8\,m/s$ and $2.44\,m/s$, $Kn = 0.14$

Figure 4. Y-velocity contours for upward and downward-moving beam at $0.8\,m/s$ and $2.44\,m/s$

Figure 4 shows the velocity magnitude of flow around both the downward and upward moving beams. The maximum fluid velocity for the downward moving beam at speed $0.8\,m/s$ is $17\,m/s$ and $12\,m/s$ for the upward moving beam. On the other hand, the highest velocity of $104\,m/s$ is seen at the corner below the beam for the downward moving beam at speed $2.44\,m/s$ whereas the highest velocity of fluid is only $27\,m/s$ for the upward moving beam.
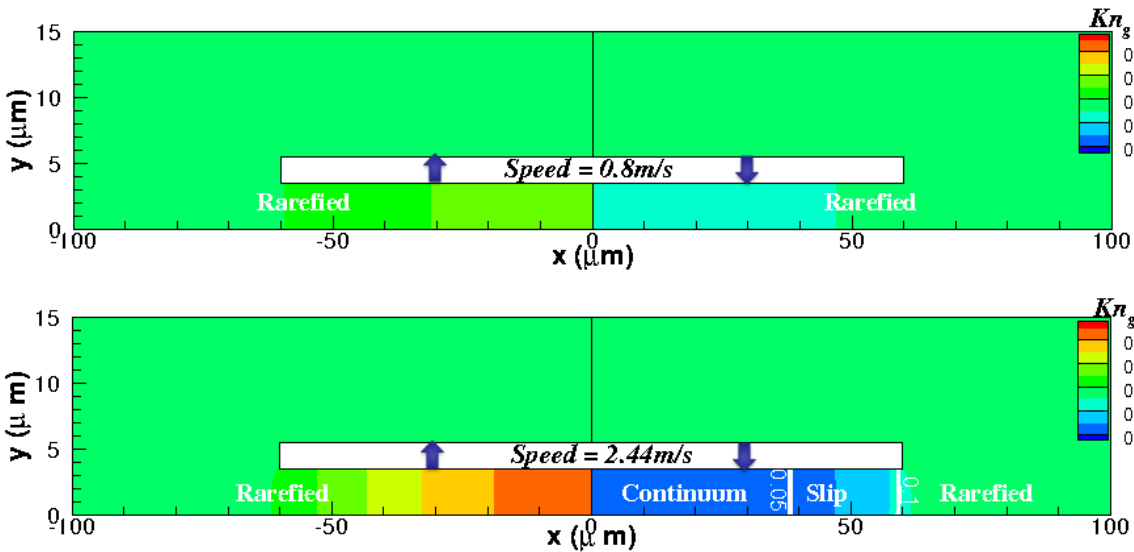
Figure 5. Kn based on gap size for upward and downward-moving beam at $0.8\,m/s$ and $2.44\,m/s$

The degree of compression and rarefaction can be understood in terms of the local Knudsen number based on characteristic length of gap-size. As shown in Fig. 5, the

range of Knudsen number for upward and downward moving beams at $V = 0.8\,m/s$ is 0.105 to 0.185. However this range is much larger for the case of the higher velocity. Contours of Knudsen number based on local mean free path and gap size, as shown in Fig. 5, indicate different regions of rarefaction relative to the entropy generation rate parameter. The use of a constant geometrical dimension to define the Knudsen number length scale fails to capture the flow gradients which are responsible for the nonlinear effects on convergence rates. Note that regions of large gradients are not the only place for rarefied flows to exist, as even a zero bulk fluid velocity at low enough pressure could be rarefied. Defining Kn based on a constant length scale is therefore more representative of the local pressures and temperatures and is well-suited for categorizing the free stream gas.

5.1. Effect of Direction of Motion on Damping Force

Beam velocity effects on the pressure field and resulting damping force predictions are performed using the nominal spatial mesh of 50×50 and velocity mesh of $10 \times 10 \times 10$.
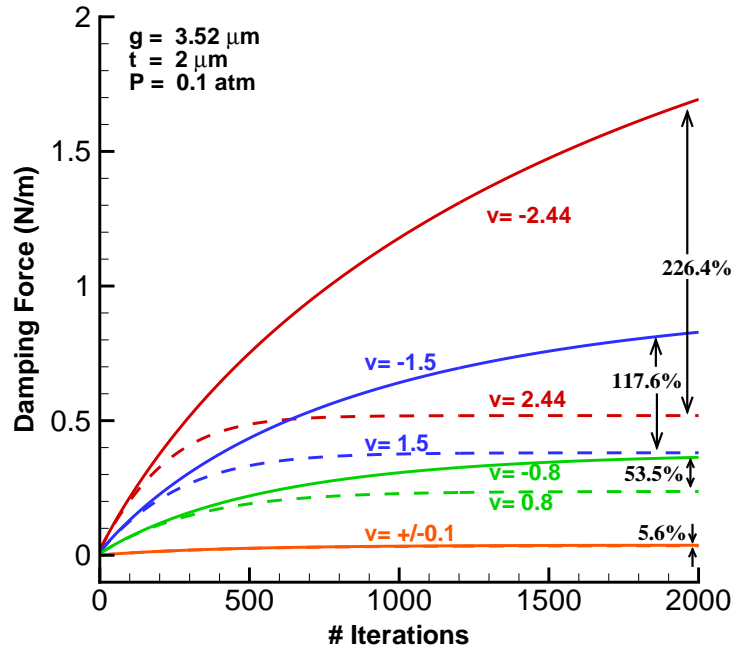

Figure 6. Damping force comparisons for varying beam velocities at $0.1\,atm$ ambient pressure

Effect of Velocity Magnitude on Damping Force   It may be observed from Fig. 6 that the damping force magnitudes range from approximately 0.05 to more than $1.7\,N/m$. The figure also depicts the % differences between upward and downward moving beam damping forces $|F/F_{up} - 1| \times 100$ for a range of velocities between 0.1 and $2.44\,m/s$.

At lower beam velocities, the differences between the upward moving beam's damping force and the downward moving beam's damping force are approximately 5%. As the beam velocity magnitude increases these differences increase to over 200% for a beam velocity of $2.44\,m/s$. Such large differences cause problems since most damping models [2, 3, 9] assume: (1) equal damping forces regardless of the direction of beam motion and (2) a linear relationship between damping force and beam velocity.

Effect of Velocity Direction on Damping Force Comparison of nondimensionalized static pressure contours $|P - P_0|/P_0$, where P_0 is the ambient pressure of $0.1\,atm$, along with streamlines shown in Fig. 7(a) for upward- and downward-moving beam reveals similar profiles. As would be expected from the damping forces shown in Fig. 6, the pressures are several times larger for the downward-moving beam. The streamlines indicate simple flow structures moving away from the high-pressure region in front of the beam towards the low-pressure region behind it. No recirculation zones are observed under these conditions, however they may begin to appear at higher pressures and velocities.
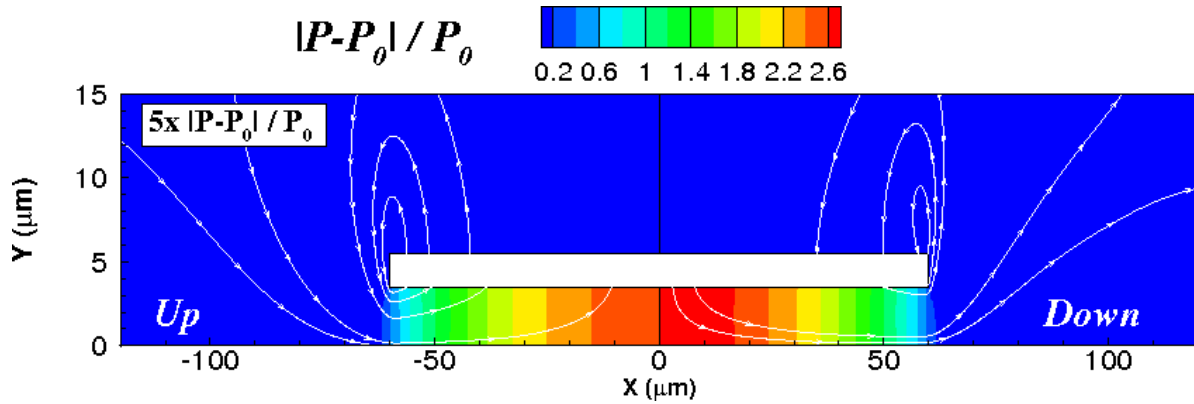
(a) Non-dimensional pressure fields
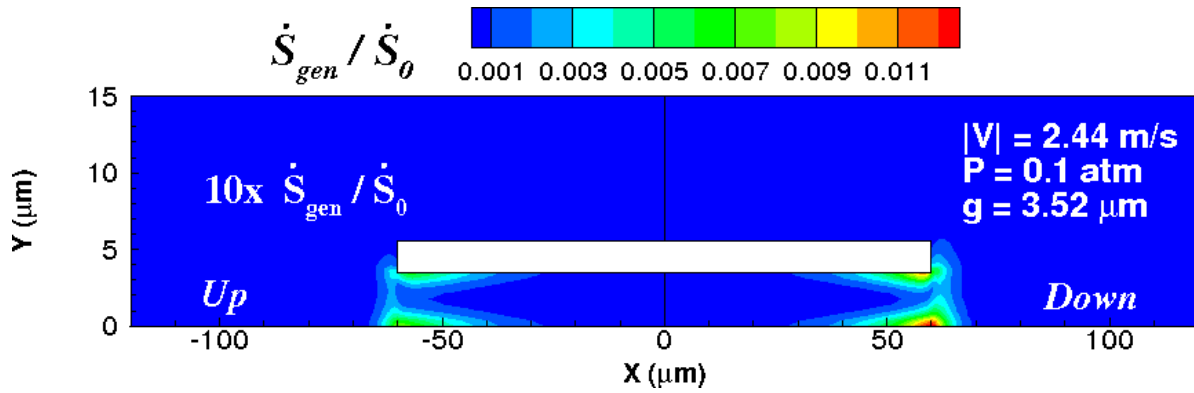
(b) Non-dimensional entropy generation rate

Figure 7. Non-dimensional properties for upward- and downward-moving beam at $2.44\,m/s$

Effect of Velocity Direction on Convergence Rate Convergence rates are also much slower for downward moving beams at higher velocities; with $14,000$ iterations required for a beam velocity of $-2.44\,m/s$. Convergence rate differences are observed as a result of the non-linearity present in the collision term of the ES-BGK equation. In particular, the coupling between the collision term and the convective term is more significant in regions of large density gradients due to larger collision frequency. Another way to explain the convergence issues for downward moving beams at higher velocities is through observations of entropy generation rate.

The entropy generation rate is a useful property which may be used to determine local regions of non-equilibrium [18]. Large flow gradients are therefore represented by large entropy generation rates, and these gradients lead to the nonlinear coupling. Figure 7(b) indicates larger entropy generation rates for the downward-moving beam at $-2.44\,m/s$ in the areas near the beam tip. The upward-moving beam has the same profile but is orders of magnitude smaller. Note in the figure the upward moving beam is shown with 10 times the entropy generation rate as actually computed.

Rarefaction Effects The differences in damping forces for upward and downward moving beams are also strongly affected by the degree of rarefaction. For an increasing Knudsen number based on the gap size and ambient gas properties, the damping force difference is also increased as is shown in figure 8.
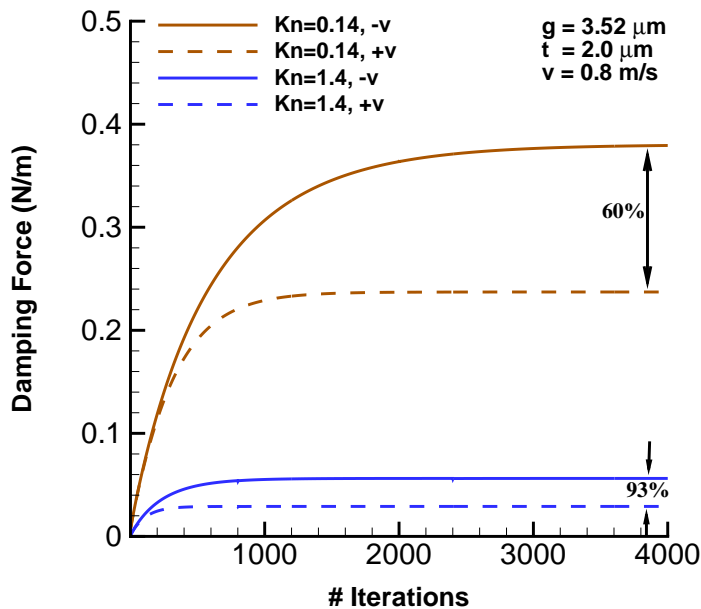

Figure 8. Damping force and comparisons for varying Kn at $0.8\,m/s$

In Fig. 9 we compare damping force from our simulations with three linear models: (i) the model based on Boltzmann-ESBGK simulations [9] (ii) a model based on unsteady Reynolds equation [2] and (iii) a model based on a modified Reynolds equation with the first-order slip boundary conditions formulated from DSMC simulations [3]. The draw back with all these models however is the inherent linearity assumption. Our simulations for upward motion of beam closely follows Guo's ES-BGK Model which was developed from 50 numerical simulations for different Kn and beam aspect ratio conditions for a velocity of $+1\,m/s$. It can be clearly seen that the damping force for a down-ward moving beam is in-fact highly non-linear with respect to velocity magnitude. The data points on the plot are at $Kn = 0.14$ and the mesh size is 50×50. The velocity mesh is maintained at $10 \times 10 \times 10$.
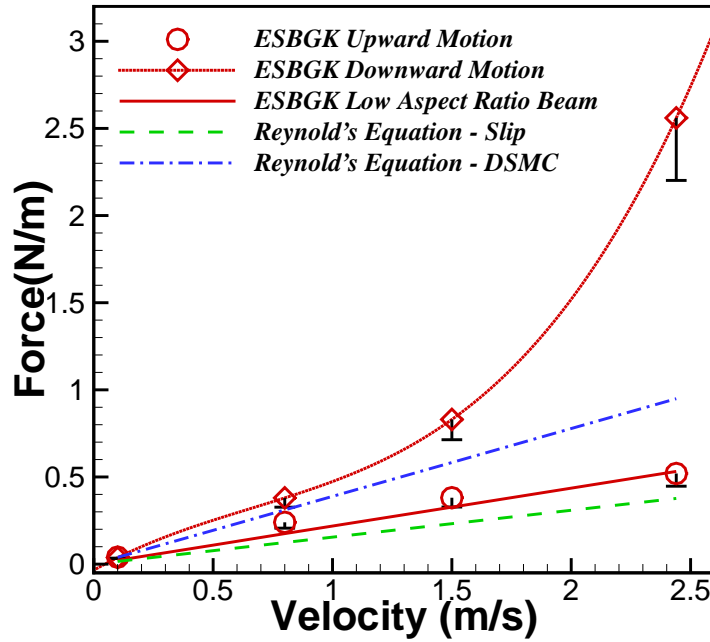
Figure 9. Damping force for upward and downward moving beam simulations at different velocities and comparison with the linear models: ES-BGK compact model for low aspect ratio beam [9], Veijola Reynolds equation with slip model [2] and Gallis-Torczynski Reynolds Equation-DSMC model [3]

Comparison with Experimental Measurements   Qualitative comparison with experimental measurements for a capacitive RF MEMS shunt switch at $1.0\,atm$ pressure in Ref. [10] shows a similar trend. Figure 6 of Ref. [10] shows the profiles of gap *vs* time for the opening and closing cycle which are reconstructed from capacitance measurements. Figure 8 of Ref. [10] shows the profiles of extracted gas damping force vs gap are shown as well as theoretical model predictions. The measured damping force coefficient is higher during the closing of the switch as compared to the opening, especially at small gaps.

Based on the data in these two graphs, we estimate that at a gap equal to $z = 0.55\mu m$, the speed of the beam during opening and closing is equal to approximately $0.009\,m/s$ and the difference in damping force is about 30%.

This is the same trend as observed in our simulations. There are notable differences in the geometry of the moving microstructure. In particular, the movable membrane in the capacitive switch of Ref. [10] has etch holes creating an overall three-dimensional structure, whereas we consider a generic planar microbeam. More significantly, the aspect ratio of the fluid gap is significantly higher in the experiments. In particular, at the point of equal speeds (gap of 0.55 microns) the aspect ratio is over 600 creating an extremely narrow fluid region. This is about an order of magnitude larger than the gap aspect ratio in the planar simulations of this work that were based on the geometry of PRISM center switch [22]. It is expected that the non-linearity effect would be more pronounced at large gap aspect ratios with an onset occurring even at smaller velocities.

6. Conclusions

Non-linear effects in the dependence of gas pressure and damping force as a function of microbeam velocity are studied by numerical simulations based on the Boltzmann-ESBGK equation. At lower beam velocities, the difference between the damping forces on upward and the downward moving beams is below about 5%. As the beam velocity magnitude increases this difference increases to over 200% for a beam velocity of $2.44\,m/s$. For an increase in rarefaction, the damping force difference between upward and downward moving beams is also increased. Therefore the direction of motion of beam should be taken into account in gas damping modeling and design of MEMS devices with large displacement and large aspect ratio structures moving with velocities on the order of 1 m/s and higher.

Acknowledgments

References

[1] G. M. Rebeiz, RF MEMS: Theory, Design and Technology, Hoboken, New Jersey, John Wiley and Sons Inc, 2003.

[2] T. Veijola, Compact Models for Squeezed-Film Dampers with Inertial and Rarefied Gas Effects, J. Micromech. Microeng. Vol. 14,2004, pp.1109-1118, doi:10.1088/0960-1317/14/7/034.

[3] M. A. Gallis, J. R. Torczynski, An Improved Reynolds-Equation Model for Gas Damping of Microbeam Motion, Journal of Microelectromechanical Systems, 2004, Vol. 13 No. 4, pp. 653-659.

[4] M. Andrews, I. Harris and G. Turner, A Comparison of Squeeze-Film Theory with Measurements on a Microstructure, Sensors Actuators A, 1993 Vol. 36 pp. 79-87.

[5] H. Sumali, Squeeze-Film Damping in the Free Molecular Regime: Model Validation and Measurement on a MEMS, J, Micromech. Microeng.,2007 Vol. 17, pp. 2231-2240.

[6] A. Nayfeh and M. Younis, A New Approach to the Modeling and Simulation of Flexible Microstructures under the Effect of Squeeze-Film Damping, J. Micromech. Microeng. 2004, Vol. 14 pp. 170-81.

[7] R. Legtenberg and H. A. C. Tilmans, Electrostatically Driven Vacuum-Encapsulated Polysilicon Resonators: I. Design and Fabrication Sensors Actuators A, 1996 Vol. 45 pp. 57-66.

[8] M. J. Martin, B. H. Houston,J. W. Baldwin, and M. K. Zalalutdinov, Damping Models for Microcantilevers, Bridges, and Torsional Resonators in the Free-Molecular-Flow Regime, Journal of Microelectromechanical Systems, Vol. 17, No. 2, April 2008.

[9] X. Guo and A. Alexeenko, Compact Model of Squeeze-Film Damping Based on Rarefied Flow Simulations, Journal of Micromechanics and Microengineering, 2009, Vol. 19, No. 045026, doi:10.1088/0960-1317/19/4/045026.

[10] P. G. Steeneken, Th. G. S. M. Rijks, J. T. M. Van Beek, M. J. E. Ulenaers, J. De Coster and R Puers, Dynamics and Squeeze Film Gas Damping of a Capacitive RF MEMS Switch, J. Micromech. Microeng. Vol. 15, 2005, pp. 176184 doi:10.1088/0960-1317/15/1/025.

[11] L. H. Holway, Kinetic Theory of Shock Structure using an Ellipsoidal Distribution Function, Rarefied Gas Dynamics: Proceedings of the Fourth International Symposium, edited by J. H. de Leeuw, Academic, New York, 1965, Vol. 1, pp. 193-215.

[12] P. Andries and B. Perthame, The ES-BGK Model Equation with Correct Prandtl Number, Rarefied Gas Dynamics: Proceedings of the 22nd International Symposium, edited by T. J. Bartel and M. A. Gallis, AIP,Melville, NY, 2001, Vol. 585,pp. 30-36.

[13] L. Mieussens and H. Struchtrup, Numerical Comparison of Bhatnagar-Gross-Krook Models with Proper Prandtl Number, Physics of Fluids, 2004, Vol. 16, No. 8, pp 2797-2813.

[14] B. Shizgal, A Gaussian Quadrature Procedure for Use in the Solution of the Boltzmann Equation and Related Problems, Journal of Computational Physics,1981, Vol. 41, pp 309-328.

[15] S. R. Mathur and J. Y. Murthy, A Pressure-Based Method for Unstructured Meshes,Numerical Heat Transfer, Part B: Fundamentals, 1997, Vol. 31, No. 2,pp. 195-215.

[16] S. R. Mathur and J. Y. Murthy, Unstructured Finite Volume Methods for Multi-mode Heat Transfer, in: W. Minkowyz, E.M. Sparrow (Eds.), Advances in Numerical Heat Transfer 2, Taylor and Francis, 2001, pp. 37-67.

[17] L. Sun, S. R. Mathur and J. Y. Murthy, An Unstructured Finite Volume Method for Incompressible Flows with Complex Immersed Boundaries, Numerical Heat Transfer, Part B, 2010, Vol. 58, No. 4, pp. 217-241.

[18] S. Chigullapalli, A. Venkattraman, M.S. Ivanov and A. Alexeenko, Entropy Considerations in Numerical Simulations of Non-Equilibrium Rarefied Flows, Journal of Computational Physics, 2010,Vol. 229, pp. 2139-2158.

[19] Van der Vorst, Iterative Krylov Methods for Large Linear Systems, Cambridge Monographs on Applied and Computational Mathematics, Cambridge University Press, 2003.

[20] G. Karypis, V. Kumar, Parallel Multilevel Graph Partitioning, IPPS, pp. 314-319, 1996.

[21] S. Chigullapalli, A. Alexeenko, Unsteady 3D Rarefied Flow Solver Based on Boltzmann-ESBGK Model Kinetic Equations, AIAA Paper 2011-3993, 41st AIAA Fluid Dynamics Conference and Exhibit, Hawaii, June 27-30, 2011.

[22] A. Alexeenko, S. Chigullapalli, J. Zheng, X. Guo, A. Kovacs, D. Peroulis, Uncertainty in Microscale Gas Damping: Implications on Dynamics of Capacitive MEMS Switches, Reliability Engineering and System Safety, 2011, Vol. 96,pp. 1171-1183.